Computers and Concrete, Vol. 5, No. 4 (2008) 401-416
DOI: http://dx.doi.org/10.12989/cac.2008.5.4.401

A mixture theory based method for three-dimensional modeling of reinforced concrete members with embedded crack finite elements

O. L. Manzoli*

Department of Civil Engineering, Sao Paulo State University (UNESP), Av. Luiz Edmundo C. Coube, S/N, 17030-360, Bauru, SP, Brazil

J. Oliver

E.T.S. d'Enginyers de Camins, Canals i Ports, Technical University of Catalonia (UPC) Campus Nord UPC, Mòdul C-1, c/Jordi Girona 1-3, 08034 Barcelona, Spain

A. E. Huespe

CIMEC/Intec, Conicet, Guemes 3450, Santa Fe 3000, Argentina

G. Diaz

E.T.S. d'Enginyers de Camins, Canals i Ports, Technical University of Catalonia (UPC) Campus Nord UPC, Mòdul C-1, c/Jordi Girona 1-3, 08034 Barcelona, Spain

(Received November 1, 2007, Accepted June 1, 2008)

Abstract The paper presents a methodology to model three-dimensional reinforced concrete members by means of embedded discontinuity elements based on the Continuum Strong Discontinuous Approach (CSDA). Mixture theory concepts are used to model reinforced concrete as a 3D composite material constituted of concrete with long fibers (rebars) bundles oriented in different directions embedded in it. The effects of the rebars are modeled by phenomenological constitutive models devised to reproduce the axial non-linear behavior, as well as the bond-slip and dowel action. The paper presents the constitutive models assumed for the components and the compatibility conditions chosen to constitute the composite. Numerical analyses of existing experimental reinforced concrete members are presented, illustrating the applicability of the proposed methodology.

Keywords: finite elements; fracture mechanics; strong discontinuities; mixture theory; finite elements with embedded discontinuities.

1. Introduction

The mechanical behavior of reinforced concrete members is strongly affected by the damage caused by the formation of cracks during the loading process. In many situations, the ultimate load

* Corresponding author, E-mail: omanzoli@feb.unesp.br

capacity corresponds to a collapse mechanism caused by the formation of one or a few dominant cracks that appear when the concrete is already highly degraded by previous cracks. Therefore, in order to model the reinforced concrete behavior, it is fundamental to account for an approach that is able to describe the formation and propagation of multiple cracks in non-homogeneous solids composed of concrete and steel bars.

Finite elements with embedded strong discontinuities have acquired great relevance, in modeling fracturing processes, mainly due to the increase in robustness and stability that they provide in comparison with alternative methods. The development of an effective technique to track multiple discontinuity paths in two and three dimensional solids, also stands out (Oliver, *et al*. (2002-a) and Oliver, *et al*. (2004)). With these advances, this finite element class currently exhibits maturity to represent the complex crack growth process in reinforced concrete, so long as the effects of the steel bars are also appropriately included. These effects must reflect the contribution provided by the mechanical behavior of the steel bars, as well as the interaction phenomena between concrete and reinforcement, related to bond-slip and dowel actions.

There are presently different possibilities to take these effects into account. A *mesoscopic* scale treatment could be adopted, using homogenous solid elements of concrete and reinforcement with interfacing elements between them to model the bonding behavior. However, when real life problems of reinforced concrete structures are focused, this mesoscopic treatment requires, many times, unaffordable computational costs. Therefore, an alternative is a *macroscopic* scale treatment, where, the steel bars are considered to be embedded in the solid elements, permitting the use of coarse meshes and thus reducing computational efforts.

In this sense, the mixture theory (Truesdell and Toupin 1960) is a suitable option for modeling reinforcement at this macroscopic level. Using this theory, the effects of the fibers (steel bars) at the mesoscopic level can be added to the matrix (concrete) behavior at the macroscopic level resulting in an equivalent homogenized material. For the long fibers case, as is the case of steel reinforcement bars, a parallel mechanical mixture option can be employed, assuming that all constituents share the same strain field (or specific components of it). Then, the composite stress field can be obtained by the sum of the stresses supplied by the constitutive model of each constituent, weighted according to its corresponding volumetric fraction. In order to formulate these constitutive models, one can resort to available phenomenological models based on standard continuum theories. In this case, the Continuum Strong Discontinuity Approach (CSDA) can be used to model material failure of the composite. The resulting methodology, which combines the CSDA with the mixture theory, was initially proposed by Linero (2006) for two-dimensional analyses of reinforced concrete members with two orthogonal bundles of fibers, which led to very promising results.

The present study extends this methodology, already presented for 2D problems in Linero (2006) and Oliver, *et al.* (2008), to three-dimensional problems with an unlimited number of fiber bundles in different directions. The matrix and each fiber bundle are treated as constituents of the composite, which in turn, can be regarded as a homogenous continuum. Thus, the numerical simulation of the formation and propagation of cracks can be carried out by using finite elements with embedded strong discontinuities, within the context of the CSDA, like in homogeneous continua, where application of that approach has already been extensively studied by Oliver, *et al.* (2004, 2006, 2008).

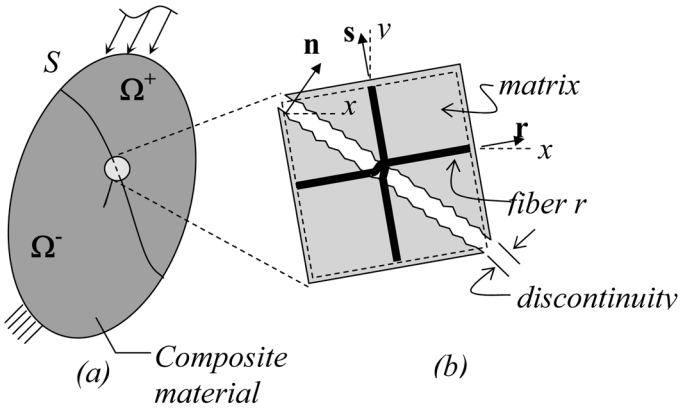

Fig. 1 (a) Composite material with one discontinuity, (b) representative material point

2. Composite material

Reinforced concrete is assumed to be a composite material made of a matrix (concrete) and long fibers (steel bars) arranged in different directions, as shown in Fig. 1.

According to the basic hypothesis of the mixture theory, the composite is a continuum in which each infinitesimal volume is occupied by all the constituents (Truesdell and Toupin 1960). Assuming a parallel layout, all constituents are subjected to the composite deformation. The composite stresses are obtained by summing up the stresses of each constituent, weighted according to their corresponding volumetric participation. Thus, the matrix strains, $\boldsymbol{\varepsilon}^m$, coincide with the composite strains, $\boldsymbol{\varepsilon}$:

$$\boldsymbol{\varepsilon}^m = \boldsymbol{\varepsilon} \tag{1}$$

The extensional strain of a fiber *f*, in direction $\mathbf{r}^{(f)}$, is equal to the component of the composite strain field in that direction, that is:

$$\boldsymbol{\varepsilon}^{(f)} = \mathbf{r}^{(f)} \cdot \boldsymbol{\varepsilon} \cdot \mathbf{r}^{(f)} \tag{2}$$

As it will be shown later, in order to take the dowel action into consideration, the fiber shear strains, $\gamma^{(f)}$, are obtained as the shear components of the composite strain field. In a local orthogonal reference system ($\mathbf{r}^{(f)}$, $\mathbf{s}^{(f)}$, $\mathbf{t}^{(f)}$) these shear components are given by:

$$\gamma_{rs}^{(f)} = 2\mathbf{r}^{(f)} \cdot \boldsymbol{\varepsilon} \cdot \mathbf{s}^{(f)} \tag{3}$$

$$\gamma_{rt}^{(f)} = 2\mathbf{r}^{(f)} \cdot \boldsymbol{\varepsilon} \cdot \mathbf{t}^{(f)} \tag{4}$$

The stresses of a composite with *nf* fibers (or fiber bundles) oriented in different directions $\mathbf{r}^{(f)}$ (*f*=1, 2, .., *nf*) can be obtained using the following weighted sum of each contribution:

$$\boldsymbol{\sigma} = k^m \boldsymbol{\sigma}^m(\boldsymbol{\varepsilon}^m) + \sum_{f=1}^{nf} k^{(f)} \{ \boldsymbol{\sigma}^{(f)}(\boldsymbol{\varepsilon}^{(f)})(\mathbf{r}^{(f)} \otimes \mathbf{r}^{(f)}) + 2\boldsymbol{\tau}_{rs}^{(f)}(\gamma_{rs}^{(f)})(\mathbf{r}^{(f)} \otimes \mathbf{s}^{(f)})^s + 2\boldsymbol{\tau}_{rt}^{(f)}(\gamma_{rt}^{(f)})(\mathbf{r}^{(f)} \otimes \mathbf{t}^{(f)})^{sym} \} \tag{5}$$

where k^m and $k^{(f)}$, are the matrix and the fiber *f* volumetric fraction, respectively, $\boldsymbol{\sigma}^m$ is the matrix stress tensor, $\boldsymbol{\sigma}^{(f)}$ is the fiber normal (axial) stress, and $\boldsymbol{\tau}_{rs}^{(f)}$ are $\boldsymbol{\tau}_{rt}^{(f)}$ the shear stress components.

For the sake of simplicity, in Eq. (5), it is assumed that the normal and tangential stress components of the fibers are related to the corresponding strains by means of specific constitutive equations in a completely decoupled behaviour.

Since the composite stresses are obtained from the composite strains, the incremental form of the composite constitutive equation can be written as:

$$\dot{\boldsymbol{\sigma}} = \mathbf{C}_{tg} : \dot{\boldsymbol{\varepsilon}} \tag{6}$$

where the tangent constitutive tensor $\mathbf{C}_{tg}$ can be obtained from the incremental form of Eq. (5), as:

$$\mathbf{C}_{tg} = k^m \mathbf{C}_{tg}^m + \sum_{f=1}^{nf} k^f \{ E_{tg}^{(f)} (\mathbf{r}^{(f)} \otimes \mathbf{r}^{(f)}) \otimes (\mathbf{r}^{(f)} \otimes \mathbf{r}^{(f)}) +$$

$$4 G_{rs}^{(f)} (\mathbf{r}^{(f)} \otimes \mathbf{s}^{(f)})^s \otimes (\mathbf{r}^{(f)} \otimes \mathbf{s}^{(f)})^s + 4 G_{rt}^{(f)} (\mathbf{r}^{(f)} \otimes \mathbf{t}^{(f)})^s \otimes (\mathbf{r}^{(f)} \otimes \mathbf{t}^{(f)})^s \} \tag{7}$$

in which $\mathbf{C}_{tg}^m = \partial \boldsymbol{\sigma}^m / \partial \boldsymbol{\varepsilon}, E_{tg}^{(f)} = \partial \sigma^{(f)} / \partial \varepsilon^{(f)}, G_{rs}^{(f)} = \partial \tau_{rs}^{(f)} / \partial \varepsilon_{rs}^{(f)}$ and $G_{rt}^{(f)} = \partial \tau_{rt}^{(f)} / \partial \varepsilon_{rt}^{(f)}$ are the tangent operators for the involved constitutive relations.

3. The continuum strong discontinuity approach (CSDA)

Crack onset and growth in the composite can be modeled in the context of the CSDA, originally proposed by Simó, *et al.* (1993). Descriptions of the CSDA, as well as the details of its implementation in the context of finite elements with embedded discontinuities, can be found in references Oliver, *et al.* (1999, 2002-b, 2006) and Oliver (1996). In order to increase robustness during the non-linear computations, a symmetric formulation (kinematically consistent) combined with an implicit-explicit integration scheme presented in reference Oliver, *et al.* (2006) are used. Continuity of the crack paths between finite elements (2D and 3D) is imposed by a global tracking algorithm described in reference Oliver, *et al.* (2002-a).

4. Constitutive models

4.1. Constitutive model for the concrete matrix

The constitutive behavior of the concrete matrix is described through an isotropic damage model with distinct tensile and compressive strengths. This model belongs to the family of damage models proposed by Simo and Ju (1987) and by Oliver, *et al.* (1990).

The model is governed by the following equations:

$$\boldsymbol{\sigma}^m = \frac{q}{r} \bar{\boldsymbol{\sigma}}^m ; \; \bar{\boldsymbol{\sigma}}^m = \mathbf{C}^m : \boldsymbol{\varepsilon}^m \quad \text{(constitutive relation)} \tag{8}$$

$$f(\boldsymbol{\varepsilon}^m, r) = \tau_\varepsilon - r \leq 0; \quad \tau_\varepsilon = \alpha \sqrt{\bar{\boldsymbol{\sigma}}^m : (\mathbf{C}^m)^{-1} : \bar{\boldsymbol{\sigma}}^m} = \alpha \sqrt{\boldsymbol{\varepsilon}^m : \mathbf{C}^m : \boldsymbol{\varepsilon}^m} \quad \text{(damage criterion)} \tag{9}$$

$$\dot{q} = H^m \dot{r} \quad \text{(softening law)} \tag{10}$$

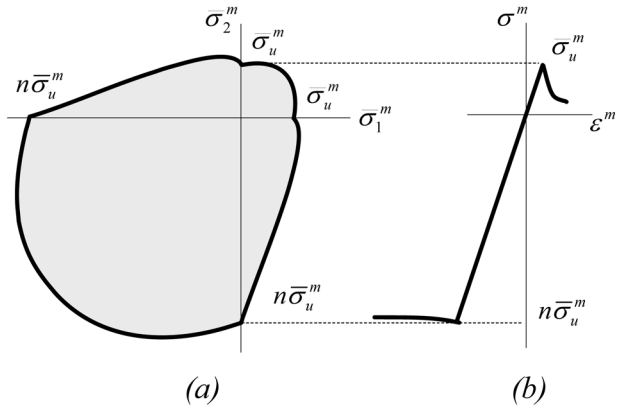

Fig. 2 Damage model: (a) damage criterion in the effective stress space, (b) one-dimensional stress-strain curve

$$r(t) = \max_{s \in [0,t]} [r_0, \tau_\varepsilon(s)] \;\; ; \;\; r_0 = \frac{\sigma_u^m}{\sqrt{E^m}} \text{ (evolution of the strain-like internal variable)} \tag{11}$$

where $\bar{\boldsymbol{\sigma}}^m$ is the effective stress tensor, $\mathbf{C}^m$ is the elastic constitutive tensor, r and q are the strain and stress-like internal variables, respectively, related in Eq. (10) through the softening modulus H^m, σ_u^m is the tensile strength and E^m is Young's modulus. The α factor, in the damage criterion of Eq. (9), is defined as:

$$\alpha = \frac{\sum_{i=1}^{3} \langle \bar{\sigma}_i^m \rangle}{\sum_{i=1}^{3} |\bar{\sigma}_i^m|} \left(1 - \frac{1}{n}\right) + \frac{1}{n} \tag{12}$$

where $\bar{\sigma}_i^m$ is the *i-th* principal effective stress; $\langle \bullet \rangle$ represents the Mac-Auley operator and n is the concrete compressive/tensile strength ratio (see Fig. 2).

The incremental form of the constitutive equation can be expressed by:

$$\dot{\boldsymbol{\sigma}}^m = \mathbf{C}_{tg}^m : \dot{\boldsymbol{\varepsilon}}^m \tag{13}$$

where the tangent constitutive tensor, $\mathbf{C}_{tg}^m$, takes one of the following values, depending on the loading status:

$$\mathbf{C}_{tg}^m = \frac{q}{r}\mathbf{C}^m \quad \text{if} \quad \dot{r} = 0 \text{ ; (unloading)} \tag{14}$$

$$\mathbf{C}_{tg}^m = \frac{q}{r}\mathbf{C}^m - \left(\frac{q - H^m r}{r^3}\right) \cdot \left[\frac{r^2}{\alpha}(\bar{\boldsymbol{\sigma}}^m \otimes \mathbf{A}) + \alpha^2 (\bar{\boldsymbol{\sigma}}^m \otimes \bar{\boldsymbol{\sigma}}^m)\right] \quad \text{if} \quad \dot{r} > 0 \text{ ; (loading)} \tag{15}$$

$$\mathbf{A} = \mathbf{C} : \partial_{\bar{\sigma}} \alpha$$

In order to make the constitutive model compatible with the regularized form of the strong discontinuity kinematics, and with the principles of fracture mechanics, the softening modulus shall depend on the strain localization bandwidth, a small regularization value k, as well as, on the

fracture energy (mode I), G_f^m. Considering this, the softening modulus H^m is assumed to be a material property that, for the linear softening case, is given by:

$$H^m = \overline{H}^m k; \quad \overline{H}^m = -\frac{(\sigma_u^m)^2}{2E^m G_f^m} \tag{16}$$

4.2. Constitutive model for the steel fibers

Steel fibers (rebars) are regarded as one-dimensional elements embedded in the matrix. They can contribute to the composite mechanical behavior introducing axial or shear strength and stiffness.

The axial contribution of each fiber bundle depends on its mechanical properties and the matrix-fiber bond/slip behavior. The combination of both mechanisms is modeled by the slipping-fiber model described below. In this framework, the dowel action can be provided by the fiber shear stiffness contribution in the crack zone.

4.2.1. Slipping-fiber model

The fiber axial contribution can be modeled through one-dimensional constitutive relations, relating extensional strains with normal stresses. The assumed compatibility between matrix and fiber strains allows for capturing the slip effect due to the bond degradation by means of a specific strain component associated with the slip. Thus, the fiber extensional strain, ε^f, can be assumed as a composition of two parts: one due to fiber mechanical deformation, ε^d, and the other related to the equivalent relaxation due to the bond-slip in the matrix-fiber interface, ε^i:

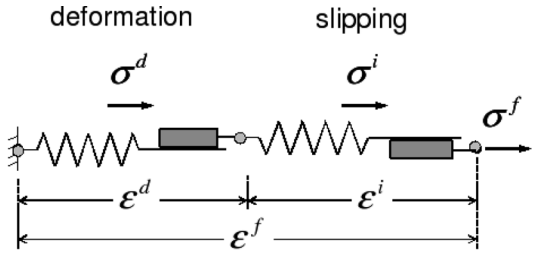

Fig. 3 Slipping-fiber model

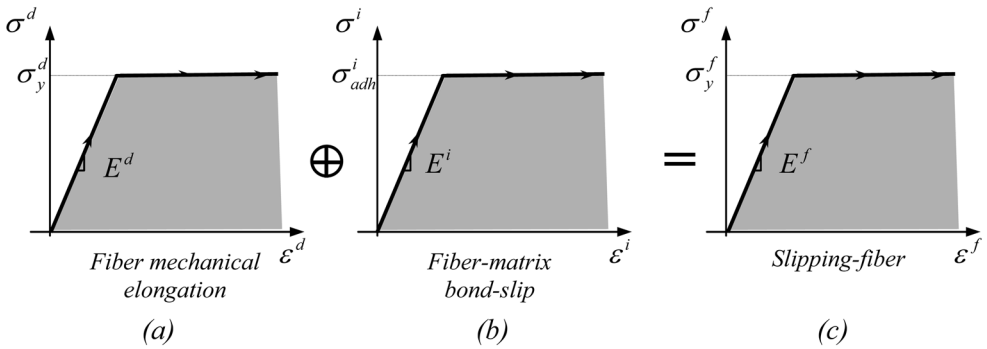

Fig. 4 Slipping-fiber model: the composition ($\oplus$) of both elements (a) and (b) must be understood as a serial mechanical system, in the sense that, deformations are additive ($\varepsilon^f = \varepsilon^d + \varepsilon^i$) and stresses are not ($\sigma^f = \sigma^d = \sigma^i$).

$$\varepsilon^f = \varepsilon^d + \varepsilon^i \tag{17}$$

Assuming a serial composition between fiber and interface, as illustrated in Fig. 3, the normal stress of the slipping-fiber model, σ^f, is equal to each component stress:

$$\sigma^f = \sigma^d = \sigma^i \tag{18}$$

The stress associated to the fiber elongation, as well as the one associated with the matrix-fiber slip effect, can be related to the corresponding strain component by means of a uniaxial linearly elastic/perfectly plastic constitutive model. Thus, this serial composition results in a slipping-fiber behavior, which can also be described by means of a linearly elastic, perfectly plastic model, whose material parameters are provided by the composition of parameters associated with each effect (see Fig. 4).

Therefore, the elastic modulus, E^f, and the yield stress of the slipping-fiber constitutive model, σ_y^f, are given by:

$$E^f = \frac{1}{1/E^d + 1/E^i} \tag{19}$$

$$\sigma_y^f = \min[\sigma_y^d, \sigma_{adh}^i] \tag{20}$$

where E^d and σ_y^d are the steel Young's modulus and the yield stress, respectively; E^i is the elastic modulus for the matrix-fiber interface and σ_{adh}^i is the bond stress limit.

The parameters related to the fiber axial deformation can be obtained from steel bar tension tests, whereas those related to the bond response can be estimated from pull-out tests.

5. Representative numerical simulations

In order to exemplify and validate the proposed approach, some numerical simulations are presented and compared with available experimental results.

5.1. Panel in tension

The reinforced concrete panel subjected to axial tension reported by Ouyang and Saha (1994) and Ouyang, *et al.* (1997), is analyzed. The specimen consists of a 686 mm × 127 mm, and 50.8 mm thick, panel, reinforced with three 5. 9 mm in diameter steel bars, as shown in Fig. 5.

The concrete mechanical properties are: E^m = 27.35 GPa, ν^m =2.0, G_f^m =100 N/m and σ_u^m =3.19

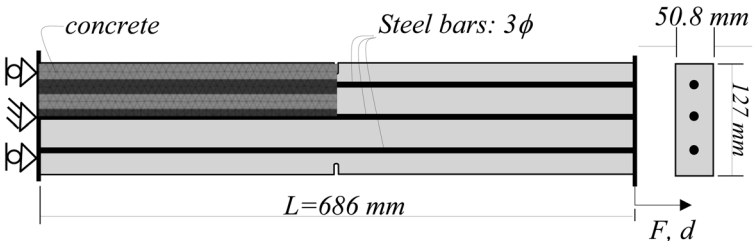

Fig. 5 Reinforced concrete panel subjected to uniaxial tension

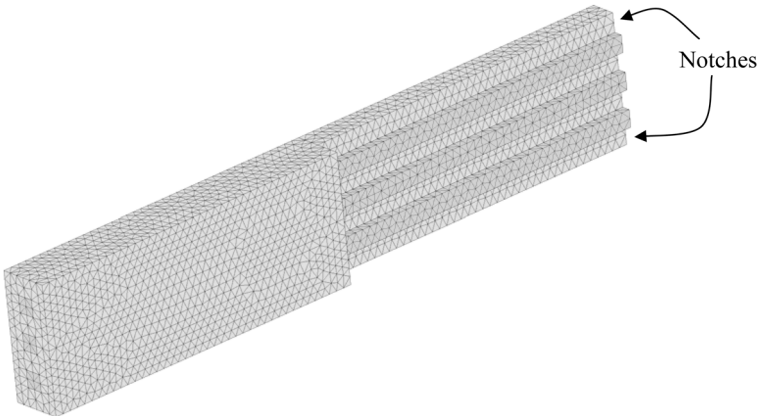

Fig. 6 Reinforced concrete panel subjected to uniaxial tension. Three-dimensional mesh with 8370 tetrahedra

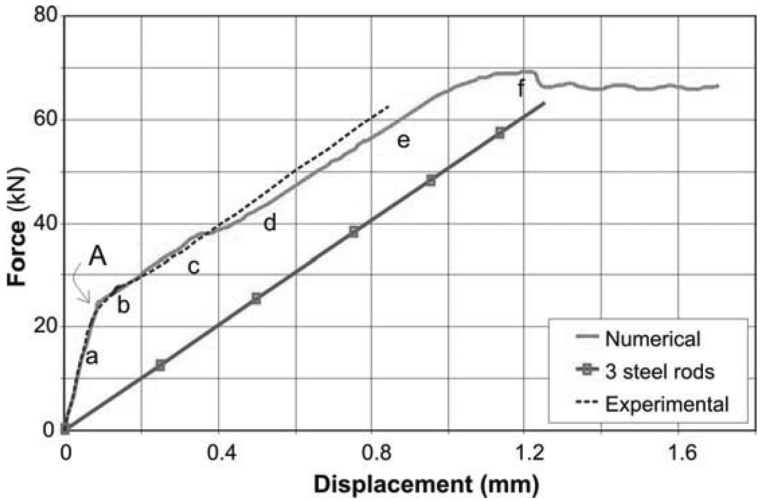

Fig. 7 Reinforced concrete panel. Reaction force vs. imposed displacement responses

MPa. The steel bars have the following properties: E^d =191.6 GPa and σ_y^d = 508 MPa.

The bond properties between concrete and steel bars were characterized through pull-out tests reported by Naaman, *et al*. (1991), which led to the following slipping-fiber model properties, described in section 4.2 : $E^f = 0.86\ E^d$ and σ_{adh}^f = 1311 MPa.

In order to compare the correctness of the present three dimensional approach, numerical analyses were carried out using 3D numerical models.

One eighth of the panel was modeled using four-node tetrahedral finite elements. Fig. 6 illustrates the used finite element mesh. The finite elements describing the composite material, made of the rebar (with a 24.71% of volumetric fraction) and the surrounding concrete are in darker colors. The rest of the panel was modeled using plain concrete properties. Axial tension was induced by imposing an increasing axial displacement at the nodes located at the right end of the panel (see Fig. 5).

The structural results (reaction force vs. imposed displacement) obtained numerically are compared with the experimental ones in Fig. 7. The obtained results resemble the experimental ones in the range

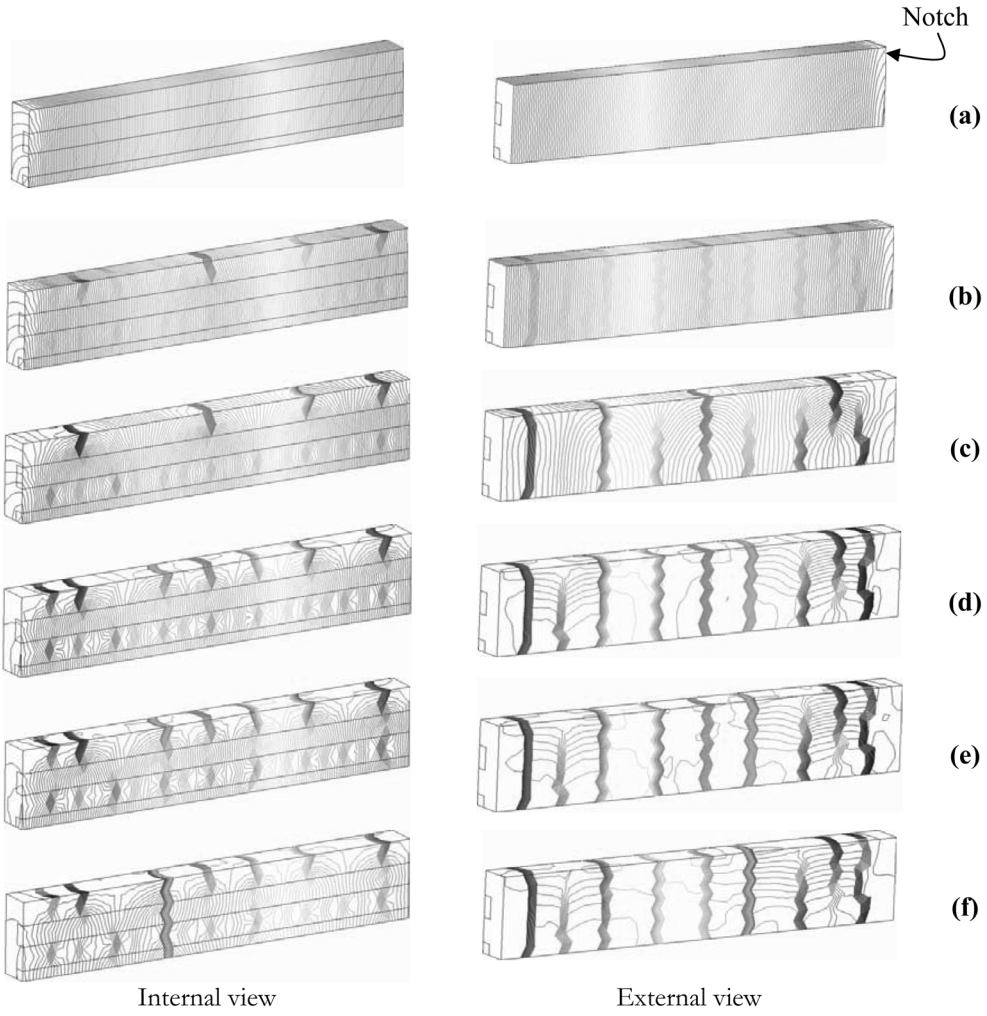

Fig. 8 Three-dimensional numerical results. Iso-displacement contours for different imposed displacement levels. Pictures **(a-f)** are in correspondence with those points displayed in Fig. 7

that these are available. It is important to note that the so called *tension-stiffening* effect is naturally captured without introducing any ad-hoc contributions associated with this phenomenon in the material constitutive model.

Fig. 8 displays the iso-displacement contours for different loading levels. In that figure, the concentrations of contour lines indicate the presence of strain localization associated with the crack opening inside the finite elements. The evolution of cracks clearly shows the distinct phases of the material degradation process. After reaching the tensile strength, the concrete begins to display cracks propagating from the external to the internal regions, until stabilization, with an almost constant spacing between them. It is important to observe that this spacing is strongly influenced by the adherence forces interacting between the concrete and reinforcement steel bar, i.e. the slipping model, as was presented in Linero (2006). And thus, naturally, it emerges a saturation crack distance as a result of the analysis that is not influenced by the finite element mesh. In this sense, the notch

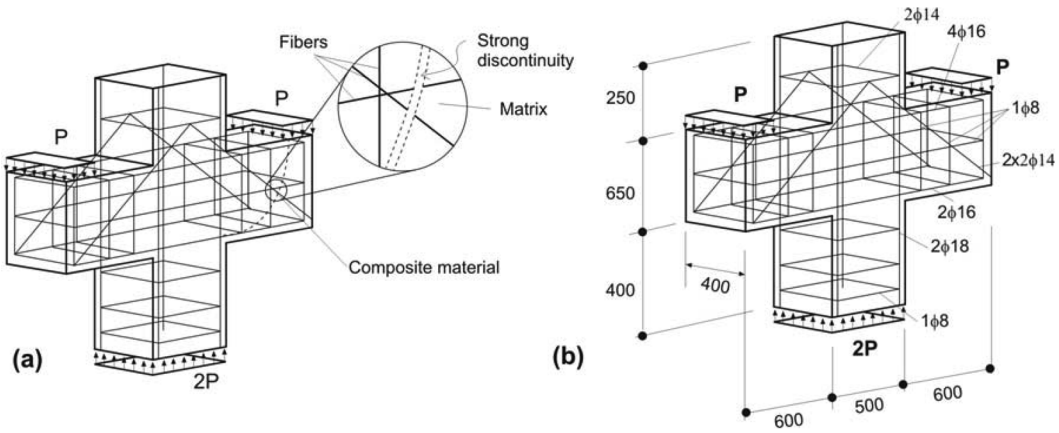

Fig. 9 Reinforced concrete corbel: **(a)**-model, **(b)** geometrical dimensions (in mm) of the simulated specimen displaying the spatial reinforcement distribution

has a marginal structural effect.

It is also possible to observe the distinct crack-opening levels at the external and internal regions (near the bars). The first cracks, almost uniformly spaced, occur when concrete reaches the tensile strength. At that moment, the structural curve in Fig. 7 shows a stiffness decrease produced by the rapid matrix degradation, whereas the steel bars remain in linearly elastic regime. As the imposed displacements are increased, new sets of cracks emerge, between the existing ones, until crack stabilization takes place. In this stabilized stage, the existing cracks open continuously. The ultimate load capacity is reached when the rebars yield at one of the cracked cross-sections, this leading to a failure mode characterized by a single active crack.

The crack spacing displayed in Fig. 8 is strongly influenced by the adherence forces intereacting between the steel reinforcement bar and the concrete, as was shown in Linero (2006). Thus, the bond-slip models in this test play a main role in order to to determine the

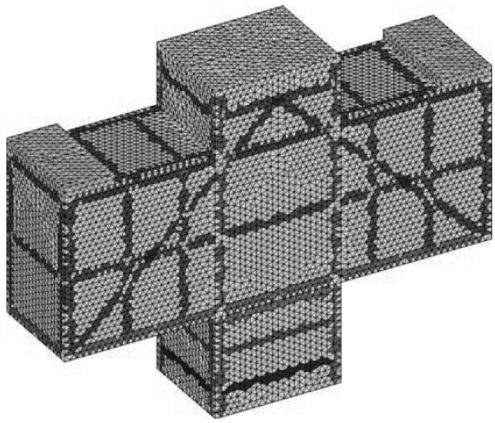

Fig. 10 Reinforced concrete corbel. Finite element mesh with 90973 tethrahedra. In colours it is observed the compound materials distribution

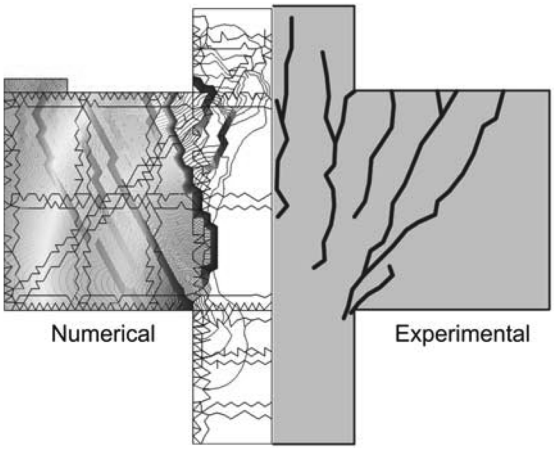

Fig. 11 Reinforced concrete corbel. Crack patterns

5.2. Reinforced concrete corbel

This typically 3D test, on a reinforced concrete corbel, carried out by Mehmel and Freitag (1967) is analyzed numerically. The test description, geometry and reinforce bar distribution, is supplied in Fig. 9. We have assumed symmetry condition; therefore, a fourth part of the structure is discretized. The finite element mesh is shown in Fig. 10.

Each rebar and the surrounding concrete were modeled as a composite material with equivalent mechanical properties. The corbel was then divided into sub-regions involving the steel bars, as shown in Fig. 10. In each sub-region, the fiber direction and volumetric fraction corresponds to the embedded steel bars in the real problem. The assumed mechanical properties for the concrete are: $E^m = 21.87$ GPa, ν^m =0.2, G_f^m =100.N/m and σ_u^m =2.26 MPa. The steel bars have the following properties: E^d =206. GPa and σ_y^d =430. MPa. The bond properties between concrete and steel bars

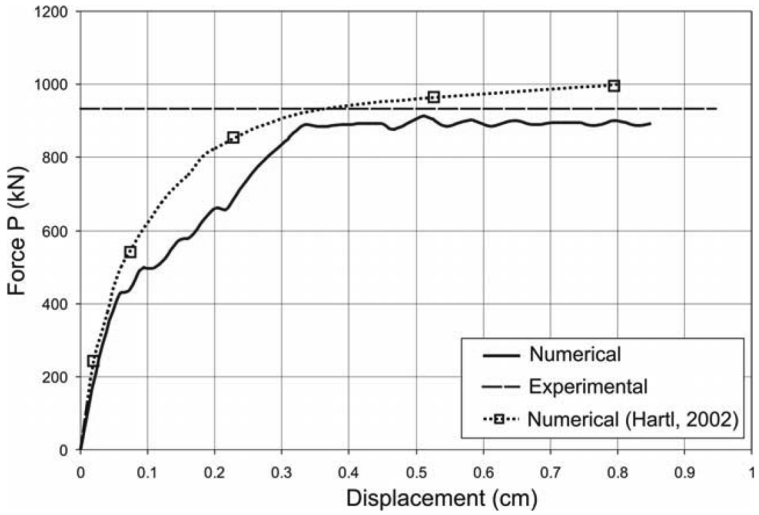

Fig. 12 Reinforced concrete corbel. Force P vs vertical displacement of the load aplication point P

were introduced taking into account the following slipping-fiber properties: $E^f=E^d$ and σ^f_{adh}=300. MPa.

It is shown in Fig. 11, left half symmetric part, the simulated crack pattern represented by the iso-displacement contours in the end of the analysis. They are in good correspondence with those observed in the experimental test, as shown in the right half symmetric part of the same figure.

Fig. 12 compares the structural action-response curves (load P vs. vertical displacement of the load application point) obtained numerically, with the proposed methodology, and the ones obtained using a model based on the smeared crack model with embedded representation of the rebars, presented by Hartl (2002). Both methodologies provide a reasonable prediction of the experimental ultimate load capacity. Although, the present one displays a well defined limit load.

5.3. Reinforced concrete beam (Leonhard's specimen)

The next example consists of one of the classical beams series reported by Leonhardt (1965), which shows the ability of the proposed methodology to predict crack patterns in heavily reinforced beams. This example, already presented in Linero (2006) and Oliver, *et al.* (2008) in a two dimensional modeling, is here tackled in a fully three dimensional context. The experimental setting is shown in Fig. 13: a heavily reinforced concrete beam, is subjected to bending/shear under a

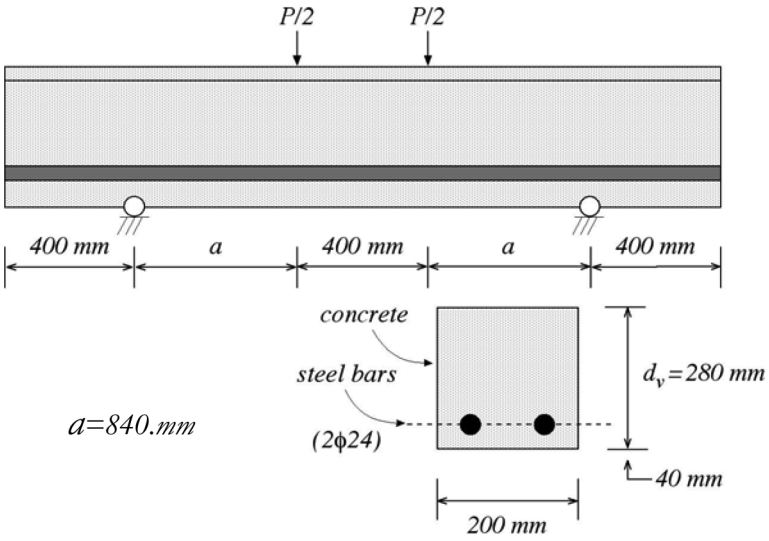

Fig. 13 Heavily reinforced beam. Problem description and model geometrical data

Table 1 Material parameters of the heavily reinforced concrete beam

Concrete				
Young's modulus E^m=20.[GPa]	Poisson's ratio ν^m=2.0	Compression strength $\sigma^m_{u(c)}$ = 20.[MPa]	Tensile strength σ^m_u = 2.[MPa]	Fracture energy G^m_f = 60.[N/m]]
Steel rebars				
Young's modulus E^d = 200.[GPa]		Poisson's ratio ν^d = 0.2	Softening modulus H^d = 0.[Gpa]	Yield stress: σ^d_y = 456.[MPa]

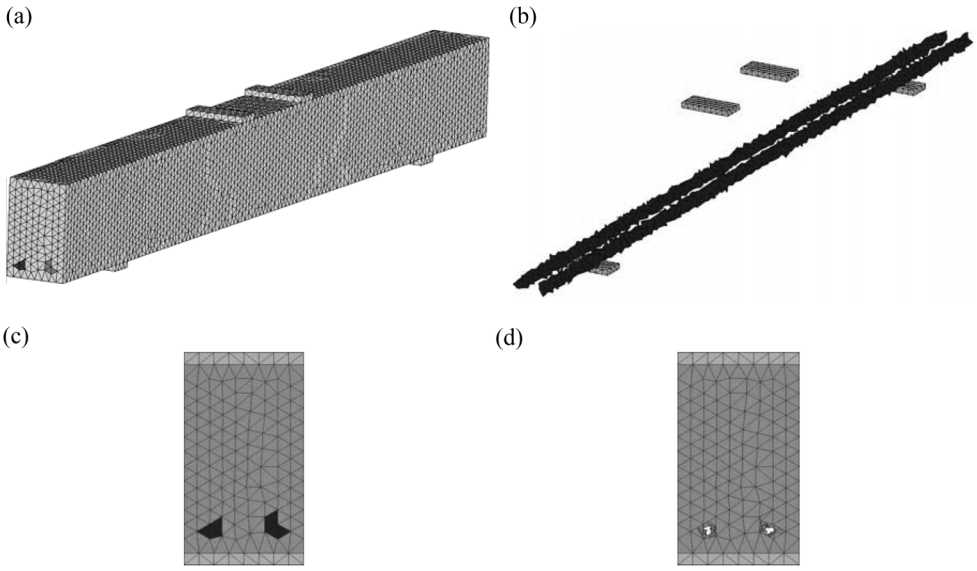

Fig. 14 Heavily reinforced beam: a) finite element mesh (57711 tetrahedra), b) composite material finite elements simulating the rebar effects, c) mesh cross section; and d) mesh cross section excluding the composite material

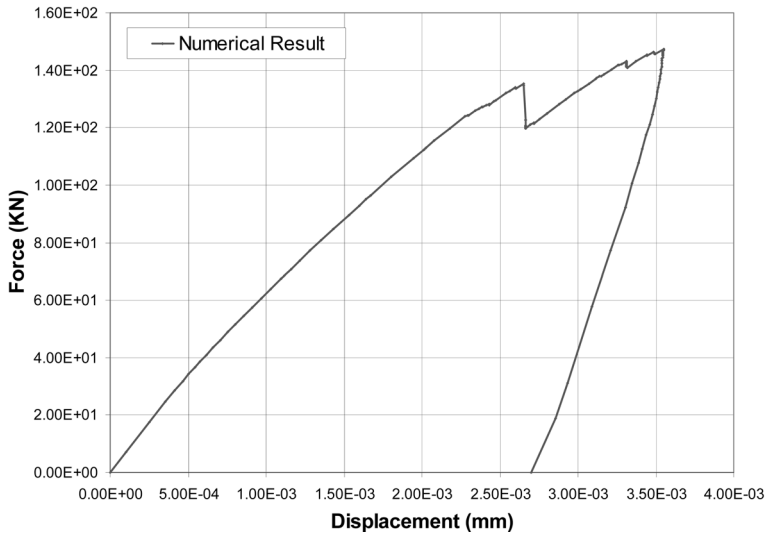

Fig. 15 Heavily reinforced beam: load P vs. load application point vertical displacement curve

couple of vertical forces, so that the central part of the beam carries pure bending (no shear force) and the remaining of the beam works under a combined bending/shear actions. The reinforcement is constituted by two longitudinal steel bars of diameter ϕ=24 mm, distributed as shown in Fig. 13.

The interface fiber-matrix model parameters are taken as: E^i =160. GPa and σ^i_{adh}=311.1 MPa. The dowel action is introduced by assuming $G^f = E^d/2(1+\nu^d)$=83.3 GPa, $\tau^f_y = \sigma^d_y/\sqrt{3}$ =263.3 MPa and perfect plasticity.

The finite element mesh is shown in Fig. 14(a). However due to the symmetry conditions, only

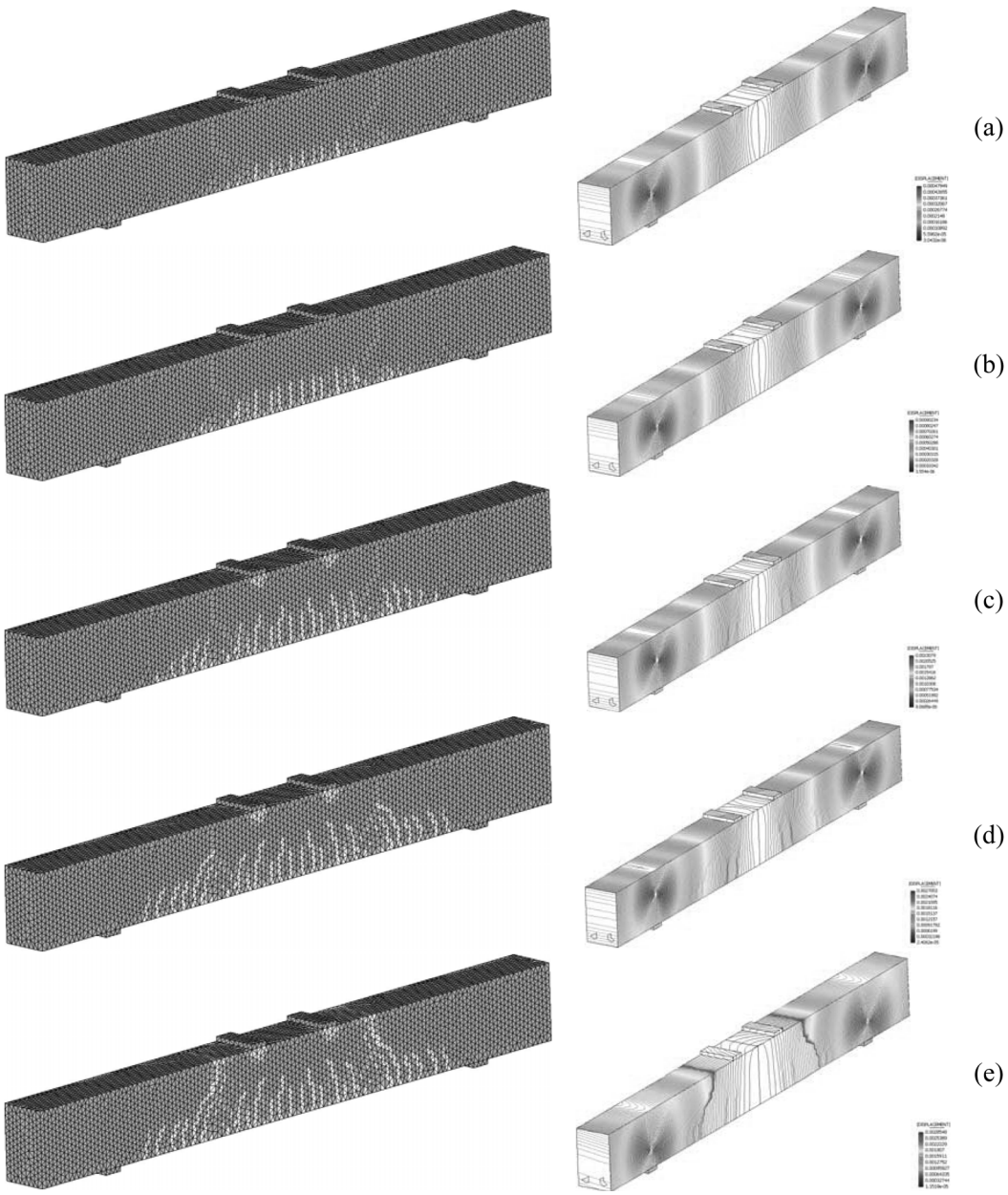

Fig. 16 Heavily reinforced beam: Evolution of the crack pattern. Damage evolution (left), showing the formed cracks; (right) contours of iso-displacements displaying the most active cracks

one half of the beam has been used in the computations. In Fig. 14(b), the set of elements made of composite material and capturing the rebar effect (with a volume fraction $k^f = 151.0$) are shown.

In Fig. 15 the obtained action-response curve is presented. As it can be observed there, the totality of the curve (pre-critical and post-critical responses) can be obtained. Before reaching the structural limit load, heavily reinforced members typically present multiple crack patterns propagating in a

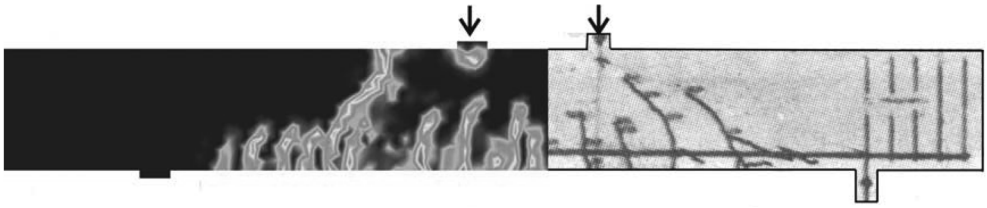

Fig. 17 shows the comparison between the numerically predicted and the experimentally obtained crack pattern for the considered beam at the end of the analysis. The numerical crack pattern is illustrated by damage contours. As it can be checked, calculated and observed crack patterns resemble fairly well

stable mode during a long period. In the post-critical regime, most of them become inactive and the collapse mechanism is characterized by one or few active cracks.

Fig. 16 illustrates the predicted evolution of the crack pattern for the simulated beam, which reproduces well the aforementioned phenomenon: at initial stages a multiple crack pattern develops from the center of the span to the end, and from the bottom to the top. In later stages, most of the vertical cracks arrest and a typical, inclined, shear/bending crack characterizes the final failure mode.

6. Concluding remarks

Along this work a methodology for three dimensional modeling of material failure in reinforced concrete members has been presented. The proposed approach tries to keep in balance the necessary complexity of a numerical model intending to capture complex phenomena, as is material failure in three-dimensional reinforced concrete structures, and the required computational cost. This is achieved by resorting to the mixture theory as a mechanical framework to include in the macroscopic scale, the effect of the rebars, without necessity of representing the mesoscopic scale at which the rebars geometrically belong.

On the other hand, the Continuum Strong Discontinuity Approach (CSDA) allows modeling the mechanical behavior of all the compounds (concrete matrix, steel rebars) and the dominant phenomena (multiple cracks patterns, bond slip and dowel effects, tension stiffening) in a fairly simple manner via standard stress-strain constitutive models. The CSDA, projects those continuum models as traction separation laws, or cohesive forces, on cracks, but that are never derived (Oliver (1996)). Indeed, this approach has evident advantages for actual three-dimensional numerical simulations

- The required finite element sizes are much larger, than those in mesoscopic approaches where the actual geometry of the rebar cross section has to be captured. Here bundles or layers of rebars, surrounded by appropriated amounts of concrete, are modeled as composite materials whose size determine that of the finite element mesh. Therefore, the required computational cost drops dramatically with respect to those mesoscopic approaches.
- On the other hand, as it has been displayed by the presented results, that simplification in the geometry does not translate into a significant loss of quality of the obtained mechanical description of the reinforced concrete members. Crack patterns, failure mechanisms and action-response curves coincide, with remarkable accuracy, with the ones displayed experiments.

References

Hartl, H. (2002), "Development of a continuum-mechanics-based toll for 3D finite element analysis of reinforced concrete structures and application to problems of soil-structure interaction", Graz University of Technology: Graz.

Leonhardt, F. (1965), "Reducing the shear reinforcement in reinforced concrete and slabs", *Mag. Concrete Res.* **17**, 187-198.

Linero, D. L. (2006), "A model of material failure for reinforced concrete via continuum strong dicontinuity approach and mixing theory", PhD Thesis, Politechnical University of Catalunya, Barcelona. Spain.

Mehmel, A. and Freitag, W. (1967), "Tragfahigkeitsversuche an Stahlbetonkonsolen", *Bauinge-nieur,* **42**, 362-369.

Naaman, A., Namur, G., Alwan, J. and Najm, H. (1991), "Fiber pullout and bond slip II. Experimental validation", *J. Struct. Eng. ASCE*. **117**, 2791-2800.

Oliver, J., Cervera, M., Oller, S. and Lubliner, J. (1990), "Isotropic damage models and smeared crack analysis of concrete", P*Proc. SCI-C Computer Aided Analysis and Design of Concrete Structures*.

Oliver, J. (1996), "Modelling strong discontinuities in solid mechanics via strain softening constitutive equations: Part 1. Fundamentals", *Int. J. Numer. Methods Eng*. **39**, 3575-3600.

Oliver, J., Cervera, M. and Manzoli, O. (1999), "Strong discontinuities and continuum plasticity models: the strong discontinuity approach", *Int. J. Plasticity*. **15**, 319-351.

Oliver, J., Huespe, A. E., Samaniego, E. and Chaves, E. W. V. (2002-a), "On strategies for tracking strong discontinuities in computational failure mechanics", *Proceedings of the Fifth World Congress on Computational Mechanics (WCCM V)*, Mang HA, Rammerstorfer FG, Eberhardsteiner J (eds), 7-12 July. Vienna, University of Technology, Austria. Page http://wccm.tuwien.ac.at

Oliver, J., Huespe, A. E., Pulido, M. D. G. and Chaves, E. V. W. (2002-b), "From continuum mechanics to fracture mechanics: the strong discontinuity approach", *Eng. Fract. Mech*. **69**, 113-136.

Oliver, J., Huespe A. E., Samaniego E. and Chaves, E. W. V. (2004), "Continuum approach to the numerical simulation of material failure in concrete", *Int. J. Numer. Anal. Methods Geomech*. **28**, 609-632.

Oliver, J., Huespe, A. E., Blanco, S. and Linero, D. L. (2006), "Stability and robustness issues in numerical modeling of material failure in the strong discontinuity approach", *Comput. Methods Appl. Mech. Eng.* **195**, 7093-7114.

Oliver, J., Linero, D. L., Huespe, A. E. and Manzoli, O. L. (2008), "Two-dimensional modeling of material failure in reinforced concrete by means of a continuum strong discontinuity approach", *Comput. Methods Appl. Mech. Eng.* **197**, 332-348.

Ouyang, C. and Shah, P. (1994), "Fracture energy approach for predicting cracking of reinforced concrete tensile members", *ACI Struct. J*. **91**, 69-78.

Ouyang, C., Wollrab, E., Kulkarni, S. and Shah, P. (1997), "Prediction of cracking response of reinforced concrete tensile members", *J. Struct. Eng. ASCE*. **123**, 70-78.

Simo, J. C. and Ju, J. W. (1987), "Stress and strain based continuum damage models: I formulation", *Int. J. Solids Struct*. **15**, 821-840.

Simo, J., Oliver, J. and Armero, F. (1993), "An analysis of strong discontinuities induced by strain softening in rate-independent inelastic solids", *Comput. Mech*. **12**, 277-296.

Truesdell, C. and Toupin, R. (1960), *The Classical Field Theories*. Handbuch der Physik, III/1, Springer. Berlín.